Theoretical study of the crystal structure, stability, and properties of phases in the V-N system

Jin Zhang,[1] Xinfeng Li,[2] Xiao Dong,[3] Huafeng Dong,[4] Artem R. Oganov,[5,*] and Jeffrey M. McMahon[6,†]

[1]*College of Education for the Future, Beijing Normal University, Zhuhai 519087, China*

[2]*Sino-French Institute of Nuclear Engineering and Technology, Sun Yat-sen University, Zhuhai 519082, China*

[3]*Key Laboratory of Weak-Light Nonlinear Photonics and School of Physics, Nankai University, Tianjin 300071, China*

[4]*School of Physics and Optoelectronic Engineering, Guangdong University of Technology, Guangzhou 510006, China*

[5]*Skolkovo Institute of Science and Technology, Skolkovo Innovation Center, 30 bldg. 1 Bolshoy blvd., Moscow 121205, Russia*

[6]*Department of Physics and Astronomy, Washington State University, Pullman, Washington 99164, USA*

(Received 14 February 2020; revised 8 July 2021; accepted 21 September 2021; published 29 October 2021)

Stable compounds in the V-N binary system are systematically investigated and four new phases are found: *Pbam*-V_5N_2, *Pnma*-V_2N, $P\bar{3}m1$-V_2N_3, and $I4/mcm$-VN_2. All the predicted high-pressure vanadium nitrides are dynamically stable at ambient pressure. Moreover, the thermodynamic stability of vanadium nitrides in the temperature range of 0–1500 K at different pressures (0, 20, 40, 60, and 120 GPa) was also evaluated within the harmonic approximation. The sequence of phases of V_2N under pressure is ε-Fe_2N type $\rightarrow$ ζ-Fe_2N type $\rightarrow$ Fe_2C type $\rightarrow$ *Pnma*-V_2N. In addition, relative stability and lattice dynamics properties of several vanadium mononitrides are systematically calculated and discussed. Structural features, mechanical properties, electronic structures, and chemical bonding of all the V-N compounds are analyzed at 0 GPa. Among these vanadium nitrides, WC-type VN has the highest Vickers hardness ($\sim$37 GPa) and superior fracture toughness (4.3–6.1 MPa $m^{1/2}$), which mainly originate from its strong V-N bonding as well as its strong three-dimensional V-N covalent bond network. The configuration of the strong and short N-N covalent bonds enables the new phase $I4/mcm$-VN_2 to exhibit good mechanical properties. Our results also reveal that the formation of a strong covalent-bond network topology in a crystal is a fundamental principle for designing a hard or superhard structure.

DOI: 10.1103/PhysRevB.104.134111

I. INTRODUCTION

Compared with pure metals, transition metal nitrides have shorter and stronger bonds, which lead to a very low compressibility and high hardness. Therefore a great deal of work has been performed to search for new transition metal nitrides (and also carbides and borides) with extreme hardness and good fracture toughness, in the hope that many of these will find applications in cutting tools and as hard coatings. Among these transition metal nitrides, vanadium nitride VN becomes an attractive candidate because of its high hardness [1,2], high melting point [3], good corrosion resistance [4], and low friction coefficient [5,6]. Based on the combination of these outstanding physical and chemical properties, vanadium nitride thin films have been fabricated to be used as hard coatings [7,8], and nanocrystalline vanadium nitride can become an attractive material for supercapacitors [9]. For example, the rocksalt-structured VN and VN-based materials are attracting interest due to their unique combination of inherently high hardness and toughness [10–12], which are unusual for ceramics.

Properties are closely related to the structure of materials. For the crystal structures of V-N compounds, it has been established that β-V_2N_{1-x} has an ϵ-Fe_2N-type ($P\bar{3}1m$-V_2N) structure and δ-VN_{1-x} has a NaCl-type structure ($Fm\bar{3}m$-VN) [13]. δ'-VN_{1-x} ($V_{32}N_{26}$) was reported to exist below 520 °C, and the lattice constant of its structure is twice as large as that of the original NaCl-type cell with six nitrogen atoms removed from the unit cell [14]. In addition, three metastable phases with stoichiometries $V_{16}N$, V_8N, and V_9N_2 have been reported [15,16] and can be formed according to a proposed metastable phase diagram [13]. Other intermediate phases, including $V_{13}N$, V_9N, and V_4N, are believed to metastably exist [16].

Much effort has been put toward exploring the structures of these stable or metastable vanadium nitrides. Even for the simple vanadium mononitride, a significant amount of attention has been paid to its crystal structure. Three decades ago, Kubel *et al.*'s [17] experiment detected that VN crystallizes in the NaCl-type structure at 298 K and transforms into a low-temperature distorted cubic phase (tetragonal, space group $P\bar{4}2m$) below 205 K. Afterwards, first-principles density functional theory (DFT) calculations [18,19] showed that NaCl-type VN is dynamically unstable at 0 K with pronounced imaginary phonon frequencies around the X point on its phonon dispersion curves. Then the explanation of the dynamical stability of NaCl-type VN at or above room

*a.oganov@skoltech.ru

†jeffrey.mcmahon@wsu.edu

temperature was sought. Ivashchenko and Turchi's DFT calculation [19] showed that an increase in temperature or nitrogen vacancies shift down the Fermi level and cause a lattice expansion, which leads to the disappearance of the imaginary phonon mode and then stabilizes NaCl-type VN. Subsequently, Ravi's calculation [20] indicated that the N vacancies in VN render the observed NaCl-type structure stable. More recently, Mei *et al.* [21], by performing both experiment and *ab initio* molecular dynamics, showed that NaCl-type VN was dynamically stabilized by the temperature-induced anharmonic effects above 250 K.

However, despite abundant theoretical and experimental studies of V-N compounds, less information was provided on the pressure-induced new compounds in the V-N system. Moreover, except for the hardness of bulk $Fm\bar{3}m$-VN (13 GPa) reported by previous experiments [22,23], the mechanical properties of other V-N compounds are still experimentally lacking due to the difficulty of preparing samples with different stoichiometries. In this work we perform a comprehensive calculation to investigate the V-N system at pressures up to 120 GPa, calculate the free energy of vanadium nitrides at finite temperatures within the harmonic approximation, analyze phase transitions and dynamical stability of high-pressure phases, estimate the elastic constants of these high-pressure phases, and then predict their hardness and fracture toughness at 0 GPa. Indeed, several new stoichiometries in the V-N system have been predicted under high pressure, and they were found to possess unusual mechanical properties.

II. COMPUTATIONAL METHODOLOGY

Stable phases in the V-N system were predicted using a first-principles evolutionary algorithm (EA) as implemented in the USPEX code [24–26] combined with *ab initio* structure relaxations using DFT with the Perdew-Burke-Ernzerhof (PBE) generalized gradient approximation (GGA) exchange-correlation functional [27], as implemented in the VASP package [28]. We also tested the DFT+U method, but the calculated enthalpies of formation from pure DFT agree better with the experimental data at 0 K from NIST-JANAF thermochemical tables [29]. The variable-composition structure searches [26] were performed for the V-N system at 0 GPa, 10 GPa, 20 GPa, 30 GPa, 40 GPa, 50 GPa, 60 GPa, 70 GPa, 80 GPa, 90 GPa, 100 GPa, 110 GPa, and 120 GPa. Several fixed-composition searches were also performed for vanadium mononitride at 0 GPa to systematically explore its possible metastable structures. We then selected the lower enthalpy phases and recalculated their enthalpies at a larger number of pressures, generating the data shown in Fig. 5. The initial generation of structures was produced randomly using space group symmetry, each subsequent generation was obtained by variation operators including heredity (40%), lattice mutation (20%), a random structure generator (20%), and transmutation (20%). The electron-ion interaction was described by the projector-augmented wave (PAW) potentials [30], with $3p^6 3d^3 4s^2$ and $2s^2 2p^3$ shells treated as valence for V and N, respectively. The plane-wave energy cutoff was chosen as 600 eV, and Γ-centered uniform k meshes with resolution $2\pi \times 0.06$ Å^{-1} were used to sample the Brillouin zone. Phonon dispersions were calculated using the finite-displacement method implemented in the PHONOPY code [31], based on the Hellmann-Feynman forces calculated with the VASP code. The Voight-Reuss-Hill approximation was adopted to estimate the polycrystalline bulk modulus (B) and shear modulus (G). The Vickers hardness was estimated according to the Chen-Niu's hardness model [32] and its modification by Tian [33], as well as Mazhnik's hardness model [34]. The fracture toughness was evaluated by Niu's fracture toughness model of covalent and ionic crystals [35] and Mazhnik's fracture toughness model [34]. The calculation of crystal orbital Hamilton population (COHP) was performed using the TB-LMTO-ASA program [36] based on the tight-binding linear muffin-tin orbital method with the atomic sphere approximation.

III. RESULTS AND DISCUSSION

A. Convex hull for V-N system

The convex-hull diagrams (Fig. 1) indicate that only $P\bar{3}1m$-V_2N and $P\bar{6}m2$-VN are the ground-state phases at zero pressure. The free energies of formation with and without including zero-point energy (ZPE) are depicted by the black solid and dash lines in Fig. 1, respectively. As we can see, taking ZPE into account did not significantly change the shape of convex hulls, especially at high pressure.

The thermodynamic stability of vanadium nitrides in the temperature range of 0–1500 K at different pressures was evaluated by constructing the thermodynamic convex hull within the harmonic approximation, which is defined using the Gibbs free energy of formation of the most stable phases for each stoichiometry, as shown in Fig. 1 [37]. Except for V_2N_3, all the other vanadium nitrides which are thermodynamically stable at 0 K keep their stability in the whole studied temperature range at these six different pressures [Figs. 1(a)–1(f)]. However, a special situation occurs at temperatures >300 K at 20 GPa; the Gibbs free energy of reaction V_2N_3 (s) → 2VN (s) + N (s) will become negative [Fig. 1(b)], which indicates that from the perspective of energy, V_2N_3 will be decomposed into VN and $P4_12_12$-N at 374 K at 20 GPa [Fig. 1(b)].

According to the calculated pressure-composition phase diagram of the V-N system (Fig. 2) at 0 K, three new compounds are found under high pressure: $I4/mcm$-VN_2 (Al_2Cu-type) appears at 33 GPa and is stable at least up to 120 GPa; $Pbam$-V_5N_2 becomes stable at 84 GPa; $Pnma$-V_2N is a new high-pressure phase of V_2N. The dynamical stability of all the V-N compounds was checked by phonon calculations (see Fig. S4 in the Supplemental Material [40]), and no imaginary vibrational frequencies are found in the whole Brillouin zone at 0 GPa, indicating all these high-pressure vanadium nitrides are dynamically stable at ambient pressure.

B. Crystal structure of V-N compounds

The optimized structural parameters of V-N compounds are listed in Table S3 in the Supplemental Materials [40]. These structures are shown in Fig. 3. Previous experimental studies reported that the NaCl-type VN transforms into a tetragonal VN (space group $P\bar{4}2m$) on cooling, and the transition

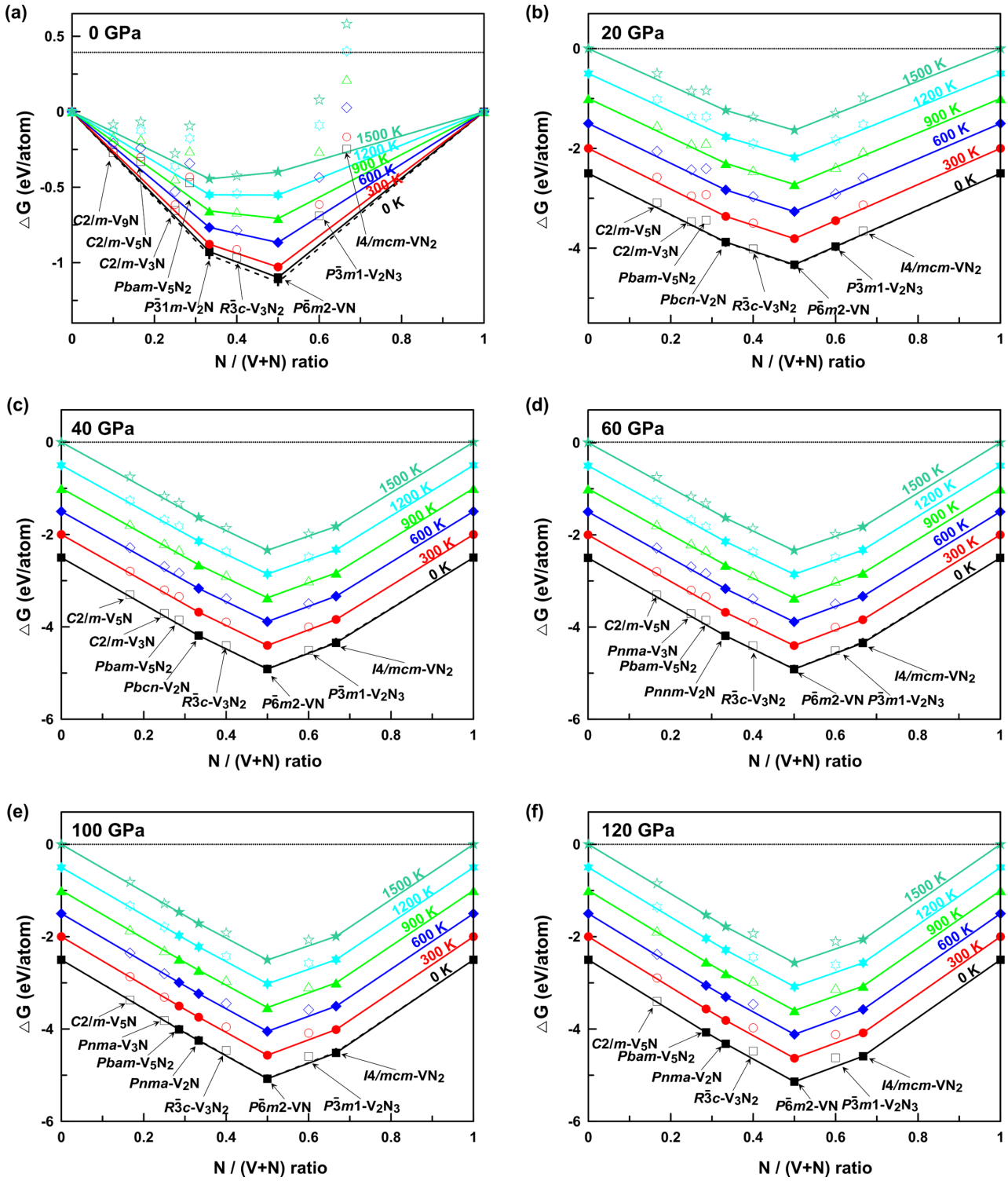

FIG. 1. Convex hulls of the V-N system in the temperature range of 0–1500 K at (a) 0 GPa, (b) 20 GPa, (c) 40 GPa, (d) 60 GPa, (e) 100 GPa, and (f) 120 GPa, respectively. The Gibbs free energy of formation with and without including zero-point energy (ZPE) are, respectively, depicted by solid and dashed back lines at 0 K. Note that the solid and dashed black convex hull really coincide at 20, 40, 60, 100, and 120 GPa. The solid symbols denote stable phases while open ones represent metastable compounds. Based on our calculations, $Im\bar{3}m$-V transforms into $R\bar{3}m$-V at 70 GPa, the phase transition sequence of N under high pressure is $Pa\bar{3} \xrightarrow{0.23\ \text{GPa}} Pbcn \xrightarrow{0.43\ \text{GPa}} P2_1/c \xrightarrow{9.5\ \text{GPa}} P4_12_12 \xrightarrow{56\ \text{GPa}} I2_13$, which is in excellent agreement with the experimental result [38] and in good agreement with the previous calculation [39]. At 0 GPa, the solid of $Im\bar{3}m$-V, α-N_2($T = 0$ K) and N_2 gas ($T > 300$ K, taking into account vibrational, translational and rotational contributions to the free energy) were used as reference state; the $Im\bar{3}m$-V and $P4_12_12$-N were adopted as reference states at both 20 and 40 GPa; the $Im\bar{3}m$-V and $I2_13$-N were adopted as reference states at 60 GPa; at both 100 and 120 GPa, the reference states were $R\bar{3}m$-V and $I2_13$-N. For clarity, the Gibbs free energies of formation in (b), (c), (d), (e), and (f) were shifted by –2.5, –2, –1.5, –1, and –0.5 eV/atom at 0, 300, 600, 900, and 1200 K, respectively.

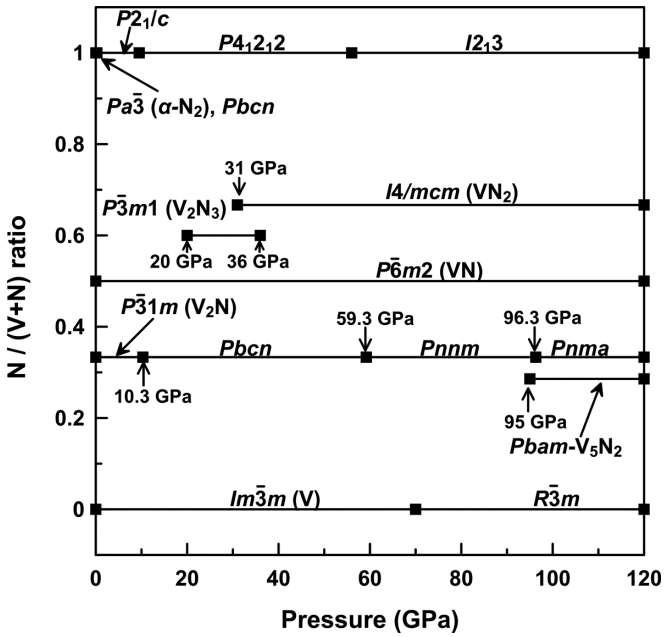

FIG. 2. Pressure-composition phase diagram of the V-N system at 0 K.

TABLE I. Relative enthalpies (taking the enthalpy of $P\bar{6}m2$-VN as reference) without and with zero-point energy (ZPE), dynamical stability (DS) for low-energy vanadium mononitrides at 0 GPa. ZPE can only be calculated for the dynamically stable phases. ΔE denotes the relative enthalpy without ZPE, and ΔE^* represents the relative enthalpy with ZPE. $\surd$ = dynamical stability; $\times$ = dynamical instability; NA = not available.

Compound	Crystal system	ΔE (meV/atom)	DS	ΔE^* (meV/atom)
$P\bar{6}m2$-VN	Hexagonal	0	$\surd$	0
$P4_2mc$-VN	Tetragonal	18	$\surd$	18
$I4_1md$-VN	Tetragonal	22	$\surd$	22
$P6_3/mmc$-VN	Hexagonal	106	$\surd$	100
$R3m$-VN	Trigonal	122	$\surd$	110
$Imm2$-VN	Orthorhombic	133	$\surd$	125
$Cmc2_1$-VN	Orthorhombic	164	$\surd$	156
$P\bar{4}2m$-VN	Tetragonal	175	$\surd$	155
$P4_2/mcm$-VN	Tetragonal	175	$\surd$	157
$P4/nmm$-VN	Tetragonal	180	$\times$	NA
$Fm\bar{3}m$-VN	Cubic	193	$\times$	NA
$Pm\bar{3}m$-VN	Cubic	679	$\times$	NA

temperature is 204 K for bulk polycrystalline VN samples [17] and 250–300 K for VN thin film [21]. However, DFT calculation indicates that hexagonal WC-type VN is the ground-state structure [41]. To our best knowledge, the WC-type VN has not been experimentally synthesized, and it is quite puzzling the experimentally reported $P\bar{4}2m$-VN is not the ground state in the framework of GGA-PBE.

One possible reason is the phase stability at finite temperature. We calculated the Gibbs free energy of different vanadium mononitrides within the harmonic approximation (HA), as shown in Fig. 4(a). The Gibbs free energy of $P\bar{4}2m$-VN is lower than WC-type VN at about 2000 K within the HA [Fig. 4(a)]. The quasiharmonic approximation (QHA), which considers the effect of the thermal expansion at finite temperature, is further used to calculate the Gibbs free energy of five tetragonal vanadium mononitrides under the temperature, as seen in Fig. 4(b). The QHA result shows that the transition temperature from $P\bar{4}2m$-VN to WC-type VN is at about 1685 K. It is reasonable to think that $P\bar{4}2$m structure is formed during high-temperature synthesis and exists metastably at lower temperature, its transition to the more favorable WC-type structure being kinetically difficult due to high energy barrier.

Another possible reason is the inaccuracy of the exchange-correlation (XC) functional. Several different exchange-correlation (XC) approximations and standard PBE (or local density approximation, LDA) corrected by Hubbard U were evaluated for the energy calculation for WC-type, NaCl-type, and $P\bar{4}2m$ phases (see Tables SI and SII in Supplemental Materials [40]). However, none of these XC approximations enable tetragonal $P\bar{4}2m$-VN to be the ground-state structure of vanadium mononitride. This reminds us of the case in CrN phase, which adopts a paramagnetic cubic structure (space group $Fm\bar{3}m$) and transforms to an antiferromagnetic orthorhombic structure (space group *Pnma*) below the Néel temperature (286 K). Then the magnetism needs to be considered for calculating the CrN structure; otherwise both the standard LDA and GGA-PBE predict WC-type phase to be the ground state of CrN [42]. Therefore the combination of magnetic ordering and the vibrational effects might be considered for predicting the experimental ground state of VN and predicting the transition temperature between NaCl-type to $P\bar{4}2m$ phase. This point has not been theoretically clarified for VN before but requires techniques beyond the present scope of this paper, such as the disordered-local-moment molecular dynamics simulations in conjunction with the temperature-dependent effective potential (DLM-MD-TDEP) [43] or special quasirandom structures (SQS) combined with spin-space averaging (SSA) [44] methods and will be therefore left for a future contribution.

In our structure searches, besides the known WC-type VN ($P\bar{6}m2$), NiAs-type VN ($P6_3/mmc$), NaCl-type VN ($Fm\bar{3}m$), and CsCl-type VN ($Pm\bar{3}m$), we also successfully found the $P\bar{4}2m$-VN which was proposed by Kubel [17]; the $P4_2mc$-VN and $I4_1md$-VN which were reported by Pu's first-principles calculation [45]; and the $P4_2/mcm$-VN and $P4/nmm$-VN that were predicted in Ivashchenko's first-principles study [19]. Moreover, new low-energy phases, $R3m$-VN, $Imm2$-VN, and $Cmc2_1$-VN, were also found. In Table I, we can see that at zero pressure the enthalpies (without ZPE) of tetragonal $P4_2mc$, $I4_1md$, $P\bar{4}2m$, $P4_2/mcm$, and $P4/nmm$ phases are all lower than that of NaCl-type phase. Slightly less stable than WC type are two structures nearly equal in enthalpy at zero pressure. One is $P4_2mc$ and the other is $I4_1md$, which crystallizes in a body-centered-tetragonal NbAs-type structure with a nonsymmorphic space group.

Except NaCl-type VN, which is dynamically unstable at zero pressure and temperature based on the theoretical analysis of its lattice dynamics [18], the dynamical stability of all the other vanadium mononitrides was checked by calculating phonon dispersions (see Fig. S5 in the Supple-

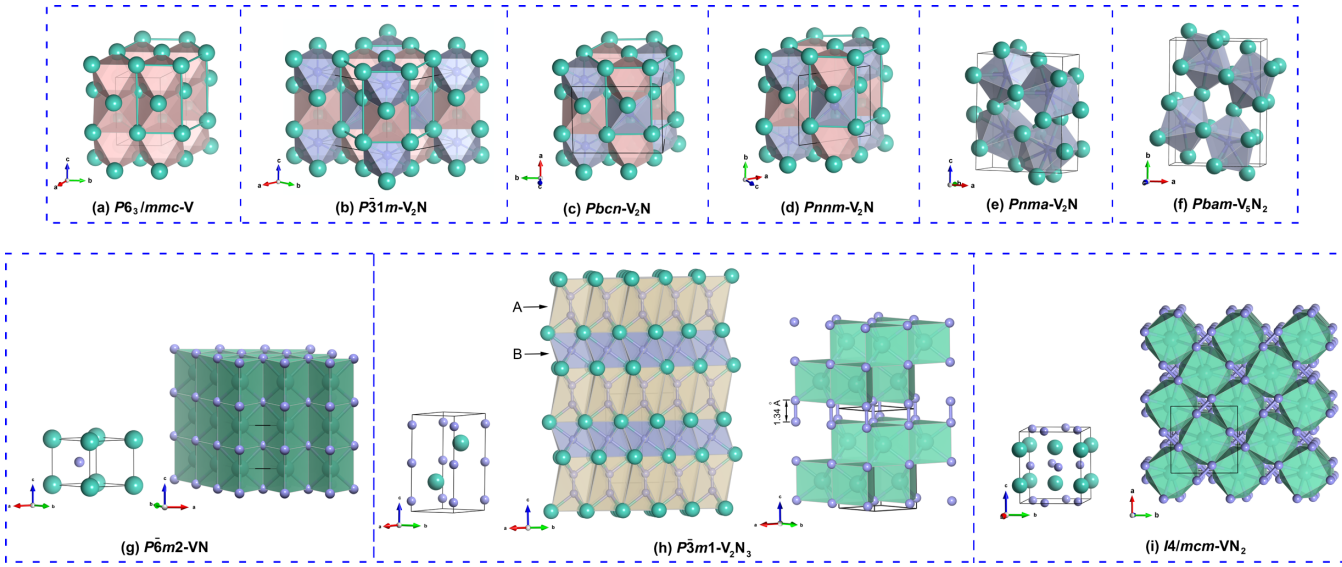

FIG. 3. Crystal structures of (a) $P6_3/mmc$-V, (b) $P\bar{3}1m$-V_2N, (c) $Pbcn$-V_2N, (d) $Pnnm$-V_2N, (e) $Pnma$-V_2N, (f) $Pbam$-V_5N_2, (g) $P\bar{6}m2$-VN, (h) $P\bar{3}m1$-V_2N_3, and (i) $I4/mcm$-VN_2. The hcp sublattices of vanadium are highlighted by green line in (a), (b), (c), and (d). Nitrogen-centered octahedra and nitrogen vacancies are shown as purple and orange polyhedra, respectively. Vanadium-centered polyhedra are shown in green. The yellow polyhedra in (h) indicate each octahedron occupied by two nitrogen atoms instead of representing the nitrogen-centered octahedra.

mental Material [40]) at 0 GPa. Imaginary frequencies are found in phonon dispersion curves of $R3m$-VN, $P4/nmm$-VN, and CsCl-type VN, indicating these three structures are dynamically unstable. Then zero-point energies (ZPEs) were calculated for the dynamically stable structures (see relative enthalpy+ZPE values in Table I). Total enthalpy sequence (including ZPE) within GGA framework for the eight dynamically stable structures is WC-type VN < $P4_2mc$-VN < $I4_1md$-VN < AsNi-type VN < $Imm2$-VN < $Cmc2_1$-VN < $P\bar{4}2m$-VN < $P4_2/mcm$-VN. Structural parameters of these vanadium mononitrides are described in more detail in the Supplemental Material.

The enthalpy-pressure relations (without ZPE) of vanadium mononitrides, calculated at the higher level of accuracy, are plotted in Fig. 5. It shows clearly that the WC-type structure is most stable up to 120 GPa, which is consistent with a previous calculated result [45]. The other two structures close in enthalpy under high pressure were $P4_2mc$ and $I4_1md$, which are 19–23 meV/atom less stable than WC type over the entire pressure range considered. In addition, considering

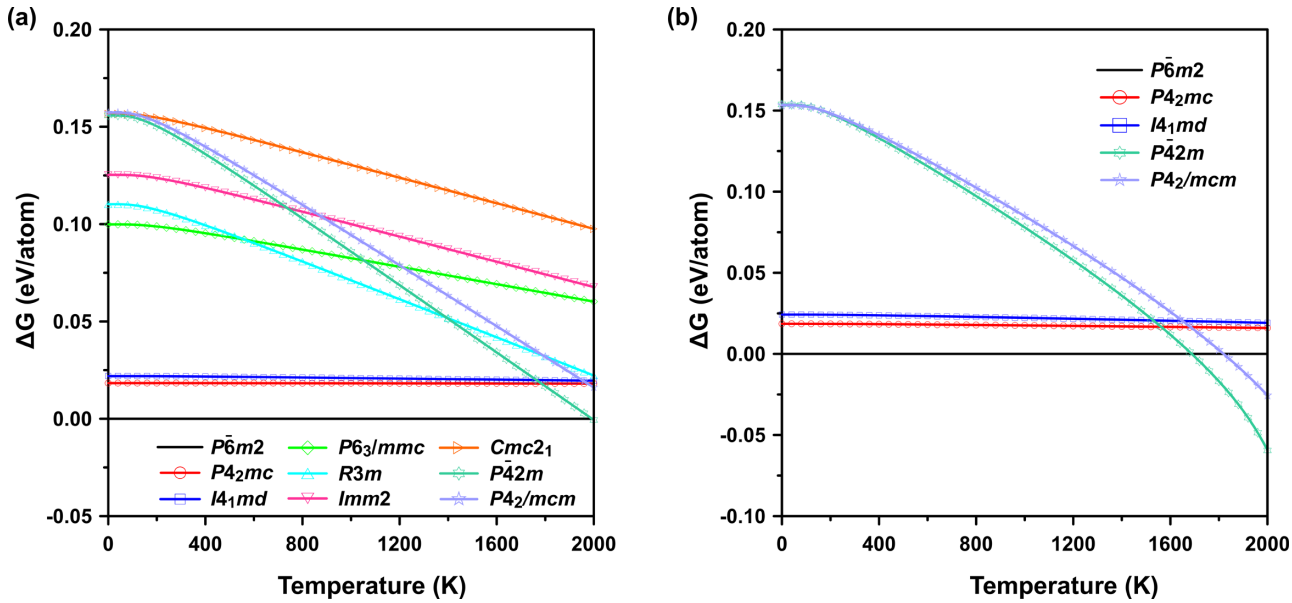

FIG. 4. Gibbs free energy as a function of temperature for (a) different vanadium mononitrides within the harmonic approximation and (b) selected tetragonal vanadium mononitrides within the quasiharmonic approximation. $P\bar{6}m2$-VN is taken as the reference.

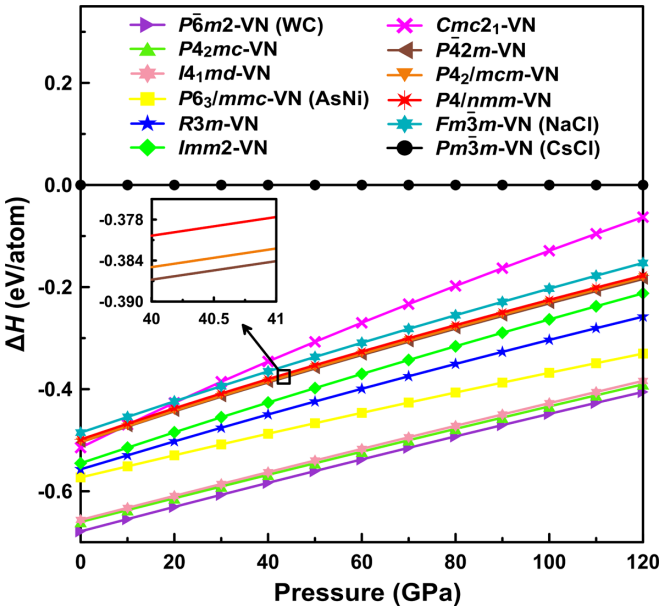

FIG. 5. Relative enthalpy as a function of pressure for vanadium mononitrides. CsCl-type VN is taken as reference. The inset shows $P\bar{4}2m$-VN, $P4_2/mcm$-VN, and $P4/nmm$-VN in an expanded pressure range from 40 to 41 GPa.

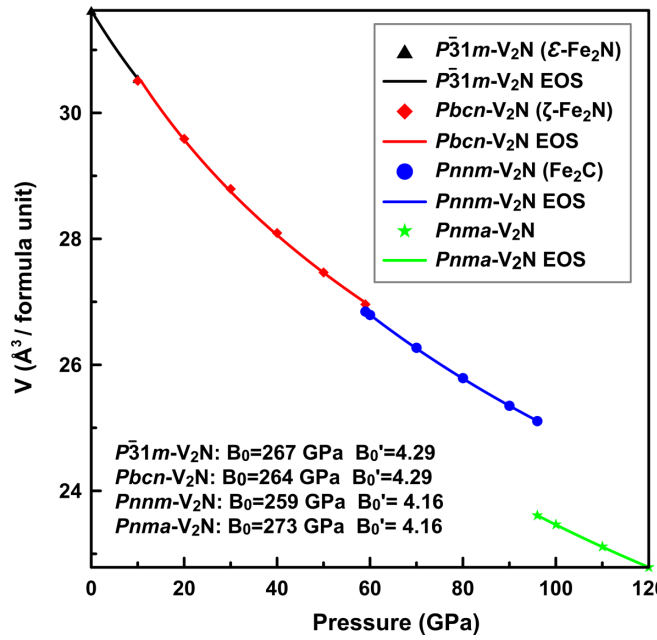

FIG. 6. Equation of state (EOS) of V_2N up to 120 GPa. The calculated pressure-volume data were fit with a third-order Birch-Murnaghan equation of state, $P(V) = (3B_0/2)[(V/V_0)^{-7/3}-(V/V_0)^{-5/3}]\{1+(3/4)(B_0'-4)[(V/V_0)^{-2/3}-1]\}$, to find B_0 and B_0'.

that $P\bar{4}2m$, $P4_2/mcm$, and $P4/nmm$ structures hold very close enthalpy, the relative enthalpy vs pressure curves for these three phases are specially inserted in Fig. 5, and it indicates that $P\bar{4}2m$-VN has lower enthalpy.

Regarding the structure of subnitride V_2N, the β-V_2N phase was observed in 1949 by Hahn [46], and later Christiansen and Lebech [47] determined the structure of this phase by neutron diffraction and showed it to be isotypical with hexagonal ε-Fe_2N (space group $P\bar{3}1m$) [13] or anti α-PbO_2 structure type. Recently, Ravi [41] performed DFT calculation to study the properties and phase stability of ζ-Fe_2N-type V_2N (space group *Pbcn*), η-Fe_2C-type V_2N (space group *Pnnm*), and CdI_2-type V_2N (space group $P\bar{3}m1$). Our calculated results show that both ζ-Fe_2N-type and Fe_2C-type V_2N are actually the high-pressure phases of V_2N and V_2N which undergo a series of structural transformations with increasing pressure: ε-Fe_2N-type V_2N first transforms into the ζ-Fe_2N-type V_2N at 10 GPa, then to η-Fe_2C-type-V_2N at 59 GPa, and then to the *Pnma*-V_2N at 96 GPa, as displayed in Fig. 6 [48]. In the ε-Fe_2N-type V_2N, ζ-Fe_2N-type V_2N, and Fe_2C-type V_2N structures, all the V atoms are three-coordinate and N atoms are six-coordinate, while the coordination numbers of V and N atoms in *Pnma*-V_2N increase to four and eight, respectively. Careful analysis shows that $P\bar{3}1m$-V_2N, *Pbcn*-V_2N, and *Pnnm*-V_2N are formed by nitrogen atoms partially occupying the octahedral interstitial sites of a vanadium sublattice, which is just slightly distorted from the perfect hcp lattice. The polyhedral representations of these V_2N structures are shown in Figs. 3(b)–3(d), and hcp vanadium [Fig. 3(a)] is drawn for comparison. The distorted hexagonal close-packed vanadium sublattice is no longer observed in the higher-pressure phase *Pnma*-V_2N [see Fig. 3(e)].

The atomic arrangement of V_2N_3 (space group $P\bar{3}m1$) is closely related to that of NiAl-type VN, which has an hcp array of vanadium with each octahedral interstice filled by one nitrogen atom. The structure of $P\bar{3}m1$-V_2N_3 can be described as an essentially hcp array of vanadium atoms, with each octahedral hole in one of the octahedral interstice layers [marked with layer B in Fig. 3(h)] occupied by one nitrogen atom, but each octahedral hole in another octahedral interstitial layer [marked with layer A in Fig. 3(h)] prefers to be occupied by two nitrogen atoms. Such manner of nitrogen occupying octahedral sites in V_2N_3 causes the stoichiometric ratio of N/V to increase from 1:1 (VN) to 3:2 (V_2N_3) and also causes a symmetry lowering from $P6_3/mmc$ (NiAs-type) to $P\bar{3}m1$. The V_2N_3 structure may also be regarded as being built of VN_6 trigonal prisms [indicated in green polyhedra in Fig. 3(h)], which link up by a short N-N bond (bond length 1.34 Å) to form a three-dimensional array.

The crystal structure of high-pressure VN_2 phase is similar to that of high-pressure TiN_2 [49]. Both of them have the anti-Al_2Cu type ($I4/mcm$) structure. This is different from the case in transition-metal borides where the Al_2Cu-type structure is often formed with a transition-metal/boron ratio of 2:1 (e.g., Ti_2B, Cr_2B, Mn_2B, Fe_2B, Co_2B, Ni_2B, and Mo_2B) [50], while the AlB_2-type ($P6/mmm$) structure is predominant for transition-metal borides with a transition-metal/boron ratio of 1:2 (e.g., TiB_2, VB_2, CrB_2, MnB_2, FeB_2, MoB_2, IrB_2) [51,52].

C. Mechanical properties of V-N compounds

The mechanical stability of vanadium nitrides was checked by calculating their elastic constants, proving that all these compounds are mechanically stable at 0 GPa based on Born criteria of mechanical stability [53]. Among them, WC-type VN has the largest elastic constants C_{33} (890 GPa) and C_{44}

TABLE II. Calculated bulk modulus B, shear modulus G, Young's modulus E, Poisson's ratio υ, volume per atom V_0, Vickers hardness H_v (H_v^c is calculated from Chen-Niu's model, H_v^t is calculated from Tian's modification model [33], H_v^m is calculated from Mazhnik's model [34]), and fracture toughness K_{IC} (K_{IC}^n is calculated from Niu's model [35], K_{IC}^m is calculated from Mazhnik's model [34]) of V-N compounds at 0 GPa, as well as literature values for $Fm\bar{3}m$-VN. G/B and υ are dimensionless; K_{IC} is in MPa m$^{1/2}$; V_0 is in Å^3/atom. Hardness, B, G, and E are in GPa.

Compound	C_{11}	C_{22}	C_{33}	C_{44}	C_{55}	C_{66}	C_{12}	C_{13}	C_{14}	C_{23}	B	G	E	G/B	υ	V_0	H_v^c	H_v^t	H_v^m	K_{IC}^n	K_{IC}^m
$Pbam$-V_5N_2	351	400	417	153	117	93	197	169		189	252	111	291	0.44	0.31	10.25	9.1	10.2	15.4	2.5	4.3
$P\bar{3}1m$-V_2N	453		441	149			162	182	26		267	142	361	0.53	0.27	10.54	14.3	14.9	17.7	2.9	4.7
$Pbcn$-V_2N	424	465	459	147	158	155	180	176		157	264	147	372	0.56	0.26	10.53	15.7	16.2	17.8	2.9	5.0
$Pnnm$-V_2N	473	419	472	145	148	180	171	147		157	257	153	383	0.60	0.25	10.52	17.7	18.0	17.8	2.9	4.4
$Pnma$-V_2N	385	450	457	153	129	130	208	188		160	267	130	335	0.49	0.29	9.82	11.9	12.7	17.1	2.7	4.7
$P\bar{6}m2$-VN	634		890	271			172	127			332	267	631	0.80	0.18	8.65	37.6	37.4	37.7	4.3	6.1
$Fm\bar{3}m$-VN	621			119			162				315	156	401	0.49	0.29	8.77	13.8	14.7	20.3	3.2	5.6
	616[a]			122[a]			165[a]				312[a]	156[a]	402[a]		0.29[a]		10-14[b,c,d]				
$P\bar{4}2m$-VN	510		510	127		127	198	198			302	138	360	0.46	0.30	8.77	11.3	12.4	18.8	2.9	5.1
$P\bar{3}m1$-V_2N_3	490		843	138		161	169	152	-11.4		300	170	429	0.57	0.26	8.60	17.7	18.3	20.4	3.2	5.1
$I4/mcm$-VN_2	631		609	168		292	212	127			311	214	522	0.69	0.22	7.71	26.8	26.9	24.8	3.6	6.6

[a]Calculated GGA result [56].
[b]Experiment [22].
[c]Experiment [57].
[d]Experiment [10].

(271 GPa), indicating its extremely high incompressibility along the c axis and great resistance to shear deformation. Bulk modulus B, shear modulus G, and Young's modulus E of V-N compounds are evaluated from the single-crystal elastic constants using the Voight-Reuss-Hill (VRH) approximation [54]. Hardness and fracture toughness are two of the most critical mechanical properties of materials. The former represents the ability of a material to resist scratching or indentation, and the latter describes the resistance of a material against crack propagation. For many applications, a material must have both high hardness and high fracture toughness. The hardnesses and fracture toughness of the polycrystalline are estimated using the empirical models [32–35]. As listed in Table II, WC-type VN possess the best combination of hardness (~37 GPa, close to the threshold of superhardness, 40 GPa) and fracture toughness ($K_{IC}^n = 4.3$ MPa m$^{1/2}$, $K_{IC}^m = 6.1$ MPa m$^{1/2}$).

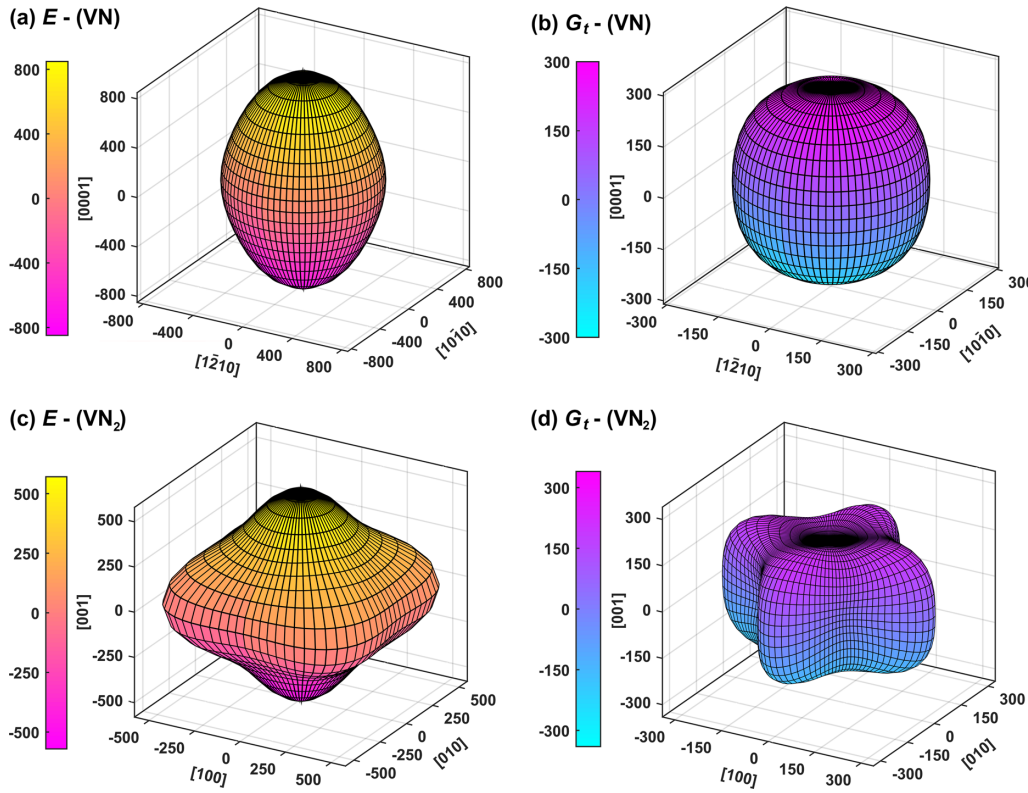

FIG. 7. Illustration of direction-dependent Young's modulus E and torsion modulus G_t for $P\bar{6}m2$-VN and $I4/mcm$-VN_2.

The second hardest V-N compound is $I4/mcm$-VN_2 (estimated hardnesses are in the range 25–27 GPa), which also has good fracture toughness with $K_{IC}^{n} = 3.6\,\mathrm{m}^{1/2}$ and $K_{IC}^{m} = 6.6\,\mathrm{m}^{1/2}$.

Pugh [55] found correlations between the G/B ratio and the ability of materials to deform plastically. Based on phenomenological observations, he proposed that materials which exhibit low G/B ratios (typically $\leqslant 0.5$) are more likely to behave in a ductile manner than materials with large G/B. From Table II, we can find that WC-type VN, $I4/mcm$-VN_2, and $Pnnm$-V_2N are brittle, while $Pbam$-V_5N_2, $P\bar{3}1m$-V_2N, $Pbcn$-V_2N, and $Pnma$-V_2N are ductile. For $P\bar{3}m1$-V_2N_3, the G/B value is 0.57. The directional dependence of Young's modulus (E) and torsional shear modulus (G_t) for the hardest vanadium nitrides is displayed in Fig. 7. The degree of elastic anisotropy in a system can be directly extracted from the asphericity of these figures. According to our results, $I4/mcm$-VN_2 has a large G/B value and exhibits remarkable elastic anisotropy of Young's modulus (E) and torsional shear modulus (G_t), while WC-type VN shows more isotropic features. The anisotropy of $I4/mcm$-VN_2 is due to its high C_{11} and low C_{13} values, resulting in a large torsional shear modulus in the axis direction and small in the diagonal direction.

D. Electronic structure and chemical bonding of V-N compounds

To further illustrate mechanical properties and determine the relative influence of various interatomic orbital interactions in vanadium nitrides, the total and projected electronic density of states (DOS), the crystal orbital Hamilton population (COHP) curves, and the integrated COHP (ICOHP) values of the ground-state V-N structures were calculated at ambient pressure [58]. From the electronic DOS at the Fermi level (E_F), it is clear that all these V-N compounds exhibit metallic behavior, see Fig. 8. For $Pbam$-V_5N_2, $P\bar{3}1m$-V_2N, $Pbcn$-V_2N, $Pnnm$-V_2N, $Pnma$-V_2N, and $P\bar{6}m2$-VN, the DOS below the Fermi levels is characterized by two regions of high DOS separated by a low-density region. The lower region arises from the hybridization of V-d and N-p states, and the upper region is dominated by V-d states. These results indicate that a hybridization between the N-p states and the V-d states occurs.

Another significant feature of the DOS is the existence of the pseudogap, which is seen as a reduction (deep minimum) in the density of states at the Fermi level. Among DOSs of all the V-N compounds, the Fermi level of $P\bar{6}m2$-VN perfectly falls into a sizable pseudogap, indicating an electronically favorable situation (the bonding states are fully occupied). This is consistent with the COHP curves of $P\bar{6}m2$-VN (see Fig. S6 in the Supplemental Material) that the pseudogap in the electronic DOS at the Fermi level indeed corresponds the separating line between the V-N bonding states below and V-N antibonding states above. Hence it is believed that there is a strong covalent bonding between the V and N atoms in $P\bar{6}m2$-VN.

ICOHP, which is the integral of the COHP up to the Fermi energy, provides a measure of the covalent-bond strength (the more negative value, the stronger the bonding strength). It should be noted that the ICOHP value does not equal the bond energy but rather only provides a reasonable estimate [59]. The previous calculation [60] has been performed to understand chemical bonding of NaCl-type VN by calculating its crystal orbital overlap population (COOP), the mechanism of which is similar to COHP in analyzing the chemical bonding. Our calculated ICOHP values are summarized in Table III [61]. Comparing the percentage of different interactions in the total bonding ("Contribution" column in Table III), we see that in all compounds, V-N interactions dominate. Besides, increasing the nitrogen content in subnitrides can improve their mechanical properties due to the formation of additional V-N bonds.

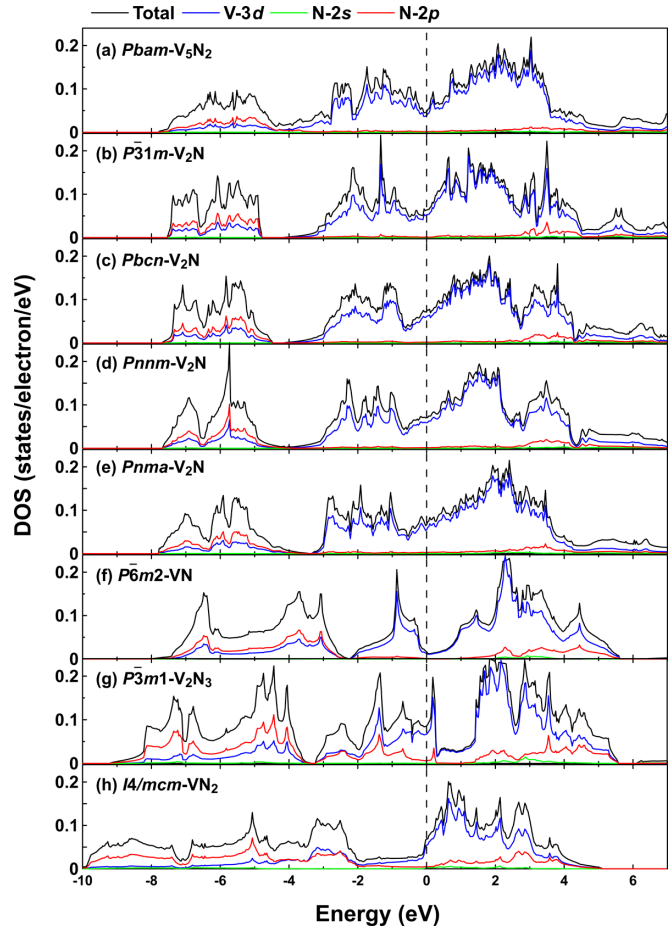

FIG. 8. Total and partial density of states for V-N compounds at 0 GPa. The Fermi level is indicated in the dashed line.

The -ICOHP values per average V-N bond of $I4/mcm$-VN_2 are the lowest (2.293 eV/pair), indicating a weakened V-N covalent bonding, which is consistent with the previous analysis in its DOS. The COHP calculation reveals a strong N-N covalent bonding (-ICOHP is 6.783 eV per average N-N pair) which offsets the negative impact of weak V-N bonding and contributes to the good mechanical properties of $I4/mcm$-VN_2. For $P\bar{3}m1$-V_2N_3, we see the largest N-N bonding strength (-ICOHP is 10.552 eV per average N-N pair) among all these vanadium nitrides, and its -ICOHP value of the average V-N pair is comparable with $P\bar{6}m2$-VN, so it could be expected to have better mechanical properties than $P\bar{6}m2$-VN. However, the bulk modulus, shear

TABLE III. Bond length ranges and average -ICOHP values for V-N compounds.

Bond type	Lengths (Å)	-ICOHP (eV/ avg bond)	n/cell	-ICOHP (eV/cell)	Contribution (%)
		Pbam-V_5N_2			
V-V	2.363–2.636	1.567	8	12.54	41.1
V-N	2.139–2.179	2.566	7	17.96	58.9
N-N	2.868	–0.066	2	–0.13	–
		$P\bar{3}1m$-V_2N			
V-V	2.760–2.857	0.267	12	3.21	28.3
V-N	1.994–1.996	2.707	3	8.12	71.7
N-N	2.835	–0.081	1	–0.08	–
		Pbcn-V_2N			
V-V	2.736–2.855	0.267	12	3.20	28.3
V-N	1.990–2.000	2.711	3	8.13	71.7
N-N	2.839	–0.026	2	–0.05	–
		Pnnm-V_2N			
V-V	2.691–2.831	0.382	12	4.58	36.2
V-N	1.987–2.019	2.689	3	8.07	63.8
N-N	2.831	–0.039	2	–0.08	–
		Pnma-V_2N			
V-V	2.473–2.618	1.535	7	10.75	39.1
V-N	2.120–2.186	2.389	7	16.72	60.9
N-N	2.830	–0.067	2	–0.13	–
		$P\bar{6}m2$-VN			
V-V	2.650–2.744	0.650	8	5.20	24.0
V-N	2.066	2.742	6	16.45	76.0
N-N	2.650	–0.063	2	–0.13	–
		$P\bar{3}m1$-V_2N_3			
V-V	2.818–2.972	0.266	9	2.39	8.1
V-N	2.032–2.048	2.743	6	16.46	56.0
N-N	1.337	10.552	1	10.55	35.9
		$I4/mcm$-VN_2			
V-V	2.488	1.206	2	2.41	8.8
V-N	2.136	2.293	8	18.35	66.6
N-N	1.383	6.783	1	6.78	24.6

modulus, and hardness of $P\bar{3}m1$-V_2N_3 are much lower than those of $P\bar{6}m2$-VN, even lower than those of $I4/mcm$-VN_2. This is due to the topology of the bond network. Although $P\bar{3}m1$-V_2N_3 has both strong V-N and N-N bonds, we can note that strong N-N bonds are only along the c axis, which implies a large value of C_{33} (consistent with the large C_{33} of $P\bar{3}m1$-V_2N_3 in Table II). For other directions in $P\bar{3}m1$-V_2N_3, we see a large reduction of its mechanical properties. In contrast, the strong N-N bonds in $I4/mcm$-VN_2 exhibit a uniform cross distribution, connecting weaker V-N bonds to form a three-dimensional, moderately strong covalent network, which improves its mechanical properties. $P\bar{6}m2$-VN, in which both the V and N atoms form simple hexagonal sublattices, has a rather isotropic distribution of strong bonds and a high hardness as a result. Therefore, for nitrogen-rich compounds, the effect of nitrogen content on the mechanical properties is minor and the atomic configuration becomes the main factor determining the mechanical properties.

IV. CONCLUSIONS

Stable V-N compounds and their crystal structures at pressures up to 120 GPa were predicted using *ab initio* evolutionary algorithm USPEX. Four new phases, *Pbam*-V_5N_2, *Pnma*-V_2N, $P\bar{3}m1$-V_2N_3, and $I4/mcm$-VN_2, were reported. Meanwhile, the enthalpy and lattice dynamics of several vanadium mononitride are systematically calculated and discussed. V_2N undergoes a phase transition from ε-Fe_2N-type($P\bar{3}1m$) to ζ-Fe_2N-type (*Pbcn*) at 10 GPa and to Fe_2C-type (*Pnnm*) *at* 59 GPa, then to *Pnma*-V_2N at 96 GPa. The phonon spectra of all these stable vanadium nitrides are calculated to verify their dynamical stability, and the Gibbs free energy at room temperature or higher temperatures is calculated to verify their high-temperature thermodynamic stability within the harmonic approximation. Except for V_2N_3 at 20 GPa, all the other vanadium nitrides are both dynamically stable and thermodynamically stable below 1500 K at all pressures studied here. Afterward, the mechanical properties (elastic constants, bulk modulus, shear modulus, Young's modulus, hardness, fracture toughness) of all the above structures were evaluated at ambient pressure. WC-type VN has the highest Vickers hardness and superior fracture toughness, and $I4/mcm$-VN_2 also exhibits good mechanical properties at ambient pressure. The electronic density of states and crystal orbital Hamilton populations of these structures were calculated, and the results showed that both the strong V-N covalent bond and the formation of a strong three-dimensional V-N covalent network are necessary for high hardness.

ACKNOWLEDGMENTS

Calculations were carried out using facilities at the Extreme Science and Engineering Discovery Environment (XSEDE), which is supported by National Science Foundation Grant No. ACI-1053575. J.Z. would like to thank the National Natural Science Foundation of China (Grant No. 12104057). J.M.M. acknowledges startup support from Washington State University and the Department of Physics and Astronomy thereat. A.R.O. thanks Russian Ministry of Science and Higher Education (grant 2711.2020.2 to leading scientific schools) for financial support. X.D. thanks the support from NSFC (Grants No. 21803033, No. 12174200), Young Elite Scientists Sponsorship Program by Tianjin (Grant No. TJSQNTJ-2018-18), Nature Science Foundation of Tianjin (Grant No. 20JCYBJC01530) and the foundation support from Laboratory of Computational Physics and United Laboratory of High-Pressure Physics Earthquake Science.

[1] G. Farges, E. Beauprez, and M. Sainte Catherine, Surf. Coat. Technol. **61**, 238 (1993).

[2] R. Sanjinés, P. Hones, and F. Lévy, Thin Solid Films **332**, 225 (1998).

[3] W. Rostoker and A. Yamamoto, Trans. Am. Soc. Met. **46**, 1136 (1954).

[4] C. Escobar, J. Caicedo, and W. Aperador, J. Phys. Chem. Solids **75**, 23 (2014).

[5] U. Wiklund, B. Casas, and N. Stavlid, Wear **261**, 2 (2006).

[6] M. Fallqvist and M. Olsson, Wear **297**, 1111 (2013).

[7] K. Kutschej, B. Rashkova, J. Shen, D. Edwards, C. Mitterer, and G. Dehm, Thin Solid Films **516**, 369 (2007).

[8] J. Caicedo, G. Zambrano, W. Aperador, L. Escobar-Alarcon, and E. Camps, Appl. Surf. Sci. **258**, 312 (2011).

[9] D. Choi, G. E. Blomgren, and P. N. Kumta, Adv. Mater. **18**, 1178 (2006).

[10] A. B. Mei, H. Kindlund, E. Broitman, L. Hultman, I. Petrov, J. E. Greene, and D. G. Sangiovanni, Acta Mater. **192**, 78 (2020).

[11] H. Kindlund, D. Sangiovanni, L. Martinez-de Olcoz, J. Lu, J. Jensen, J. Birch, I. Petrov, J. Greene, V. Chirita, and L. Hultman, APL Mater. **1**, 042104 (2013).

[12] H. Kindlund, D. Sangiovanni, J. Lu, J. Jensen, V. Chirita, J. Birch, I. Petrov, J. Greene, and L. Hultman, Acta Mater. **77**, 394 (2014).

[13] O. Carlson, J. Smith, and R. Nafziger, Metall. Mater. Trans. A **17**, 1647 (1986).

[14] T. Onozuka, J. Appl. Crystallogr. **11**, 132 (1978).

[15] D. I. Potter, H. D. Epstein, and B. M. Goldstein, Metall. Trans. **5**, 2075 (1974).

[16] G. Nouet, J. Vicens, and P. Delavignette, Phys. Status Solidi A **62**, 449 (1980).

[17] F. Kubel, W. Lengauer, K. Yvon, K. Knorr, and A. Junod, Phys. Rev. B **38**, 12908 (1988).

[18] E. I. Isaev, S. I. Simak, I. Abrikosov, R. Ahuja, Y. K. Vekilov, M. Katsnelson, A. Lichtenstein, and B. Johansson, J. Appl. Phys. **101**, 123519 (2007).

[19] V. I. Ivashchenko and P. E. A. Turchi, Phys. Rev. B **78**, 224113 (2008).

[20] C. Ravi, H. K. Sahu, M. C. Valsakumar, and A. van de Walle, Phys. Rev. B **81**, 104111 (2010).

[21] A. B. Mei, O. Hellman, N. Wireklint, C. M. Schlepuetz, D. G. Sangiovanni, B. Alling, A. Rockett, L. Hultman, I. Petrov, and J. E. Greene, Phys. Rev. B **91**, 054101 (2015).

[22] L. Toth, *Transition Metal Carbides and Nitrides* (Elsevier, New York, 2014).

[23] H. O. Pierson, *Handbook of Refractory Carbides & Nitrides: Properties, Characteristics, Processing and Apps* (William Andrew, Norwich, NY, 1996).

[24] A. R. Oganov and C. W. Glass, J. Chem. Phys. **124**, 244704 (2006).

[25] A. O. Lyakhov, A. R. Oganov, H. T. Stokes, and Q. Zhu, Comput. Phys. Commun. **184**, 1172 (2013).

[26] A. R. Oganov, A. O. Lyakhov, and M. Valle, Acc. Chem. Res. **44**, 227 (2011).

[27] J. P. Perdew, K. Burke, and M. Ernzerhof, Phys. Rev. Lett. **77**, 3865 (1996).

[28] G. Kresse and J. Furthmüller, Phys. Rev. B **54**, 11169 (1996).

[29] M. W. Chase Jr., NIST-JANAF Thermochemical Tables, 4th ed., Part I, Al-Co, Journal of Physical and Chemical Reference Data, No. 9 (American Institute of Physics, New York, 1998).

[30] P. E. Blöchl, Phys. Rev. B **50**, 17953 (1994).

[31] A. Togo, F. Oba, and I. Tanaka, Phys. Rev. B **78**, 134106 (2008).

[32] X.-Q. Chen, H. Niu, D. Li, and Y. Li, Intermetallics **19**, 1275 (2011).

[33] Y. Tian, B. Xu, and Z. Zhao, Int. J. Refract. Met. Hard Mater. **33**, 93 (2012).

[34] E. Mazhnik and A. R. Oganov, J. Appl. Phys. **126**, 125109 (2019).

[35] H. Niu, S. Niu, and A. R. Oganov, J. Appl. Phys. **125**, 065105 (2019).

[36] G. Krier, O. Jepsen, A. Burkhart, and O. K. Andersen, The TB-LMTO-ASA program, Stuttgart, 1995.

[37] Figure 1 just reflects the thermodynamical stability of the vanadium nitrides with increasing temperature at a certain pressure and does not include the information of the temperature-induced phase transition. In addition, even though the HA method is not as accurate as *ab initio* MD, we still thought it would be informative for readers, for example, readers can compare how big the impact is of the anharmonic influence for these vanadium nitrides if they have the computer resources to perform the *ab initio* MD in the future.

[38] Y. Ding, R. Ahuja, J. Shu, P. Chow, W. Luo, and H.-k. Mao, Phys. Rev. Lett. **98**, 085502 (2007).

[39] C. J. Pickard and R. J. Needs, Phys. Rev. Lett. **102**, 125702 (2009).

[40] See Supplemental Material at http://link.aps.org/supplemental/10.1103/PhysRevB.104.134111 for phonon dispersion curves, formulas for the elastic moduli, and structural parameters of V-N compounds, as well as the convex hull of V-N calculated from the GGA+U method.

[41] C. Ravi, Calphad **33**, 469 (2009).

[42] V. I. Ivashchenko, P. E. A. Turchi, V. I. Shevchenko, and E. I. Olifan, Phys. Rev. B **84**, 174108 (2011).

[43] N. Shulumba, B. Alling, O. Hellman, E. Mozafari, P. Steneteg, M. Odén, and I. A. Abrikosov, Phys. Rev. B **89**, 174108 (2014).

[44] L. Zhou, F. Körmann, D. Holec, M. Bartosik, B. Grabowski, J. Neugebauer, and P. H. Mayrhofer, Phys. Rev. B **90**, 184102 (2014).

[45] P. Chun-Ying, Z. Da-Wei, B. Dai-Xiao, L. Cheng, J. Xi-Lian, S. Tai-Chao, and Z. Fei-Wu, Chin. Phys. B **23**, 026201 (2014).

[46] H. Hahn, Z. Anorg. Allg. Chem. **258**, 58 (1949).

[47] A. N. Christensen and B. Lebech, Acta Crystallogr., Sect. B: Struct. Sci. **35**, 2677 (1979).

[48] The reason that P-V EOS is presented for V_2 N while not for VN is that we found V_2 N undergoes a series phase transition with increasing pressure, while VN shows no phase transition at pressures up to 120 GPa based on our structural searches. Therefore we only construct the equation of state for V_2 N (Fig. 6). In addition, based on the results of literature research, V_2 N does not involve disputes or confusion caused by temperature. In addition, since the temperature-related calculation is expensive, we did not present the function of temperature for V_2 N in the current paper.

[49] S. Yu, Q. Zeng, A. R. Oganov, G. Frapper, and L. Zhang, Phys. Chem. Chem. Phys. **17**, 11763 (2015).

[50] P. Mohn, J. Phys. C: Solid State Phys. **21**, 2841 (1988).

[51] A. Friedrich, B. Winkler, E. A. Juarez-Arellano, and L. Bayarjargal, Materials **4**, 1648 (2011).

[52] P. Vajeeston, P. Ravindran, C. Ravi, and R. Asokamani, Phys. Rev. B **63**, 045115 (2001).

[53] J. Nye, *Physical Properties of Crystals: Their Representation by Tensors and Matrices*, Oxford Science Publications (Clarendon Press, Oxford, England, 1985).
[54] R. Hill, Proc. Phys. Soc., Sect. A **65**, 349 (1952).
[55] S. Pugh, Philos. Mag. **45**, 823 (1954).
[56] Y. Liang, X. Yuan, and W. Zhang, Solid State Commun. **150**, 2045 (2010).
[57] S. Wang, X. Yu, J. Zhang, L. Wang, K. Leinenweber, D. He, and Y. Zhao, Cryst. Growth Des. **16**, 351 (2016).
[58] For the entire paper, we centered the discussion around the thermodynamically stable structures at different pressures, which are the eight vanadium nitrides indicated in Fig. 2. Then the density of state and COHP are only calculated for these eight structures at zero pressure.
[59] R. Dronskowski, *Computational Chemistry of Solid State Materials* (WILEY-VCH, Weinheim, 2005), Vol. 300.
[60] D. G. Sangiovanni, L. Hultman, and V. Chirita, Acta Mater. **59**, 2121 (2011).
[61] In our work, DOS is calculated using VASP and COHP is calculated using TB-LMTO-ASA. The accuracy of TB-LMTO-ASA with reference to VASP is reflected in Fig. S6 (see Supplemental Material [40]). In Fig. S6 we can see that even though the DOS and COHP of $P\bar{6}m2$-VN are calculated in different codes, they have the same Fermi energy and energy range.